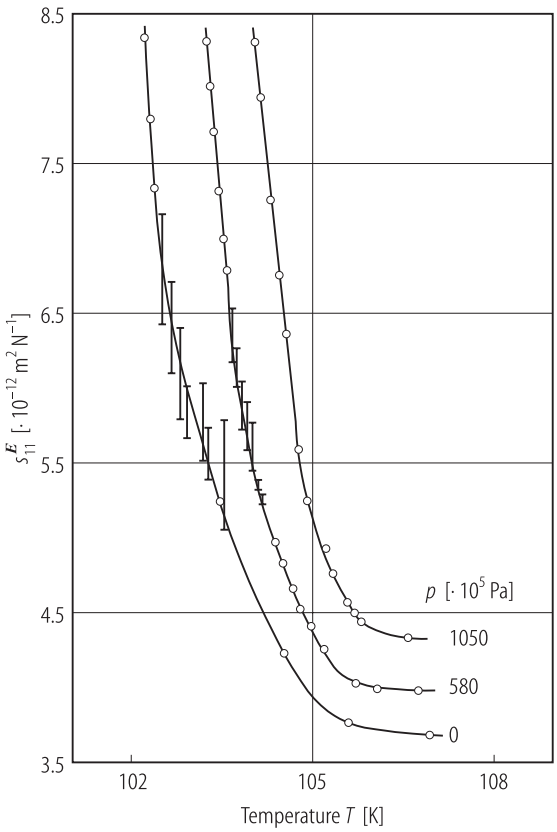

Fig. 1A-8-060. $SrTiO_3$. s. T [70Sor1]. Parameter: p. $E_{bias} = 9.35 \cdot 10^5$ V m^{-1}, $E_{ac} = 93.5$ V m^{-1}.

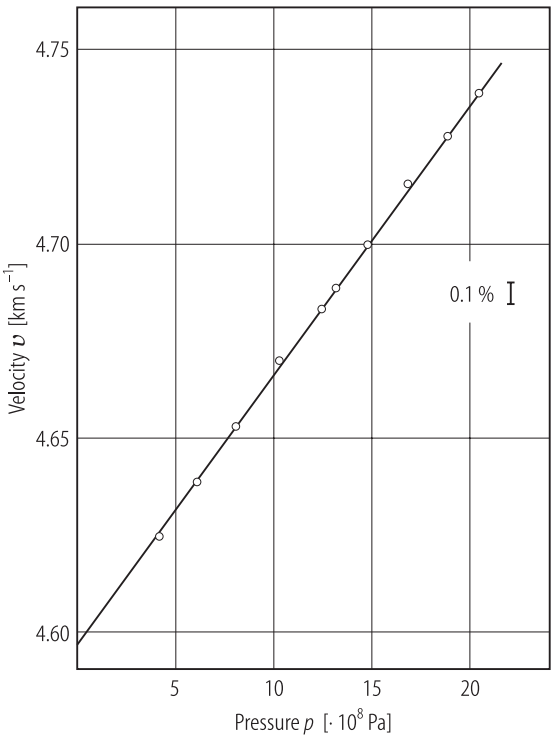

Fig. 1A-8-061. $SrTiO_3$. υ vs. p [71Bea]. υ: velocity of shear wave propagated along [110]. T = 295 K.

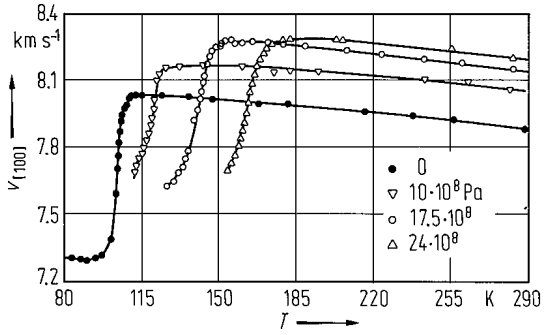

Fig. 1A-8-062. $SrTiO_3$. $v_{[100]}$ vs. T [75Oka]. Parameter: p. $v_{[100]}$: velocity of longitudinal ultrasonic wave propagated along [100].

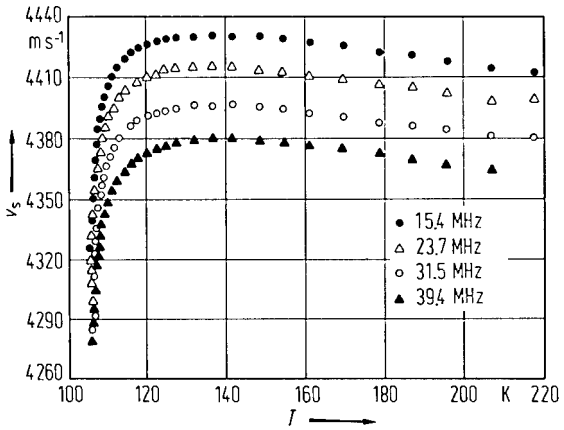

Fig. 1A-8-063. $SrTiO_3$. v_s vs. T [77Bje]. v_s: velocity of surface acoustic wave propagated in [100] direction on (001) surface. Parameter: f.

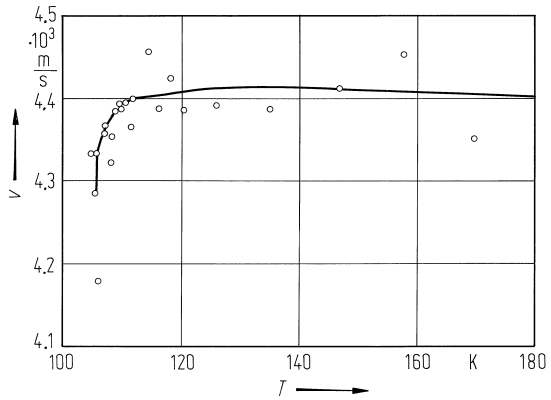

Fig. 1A-8-064. $SrTiO_3$. v vs. T [85Fos2]. v: Rayleigh wave velocity.

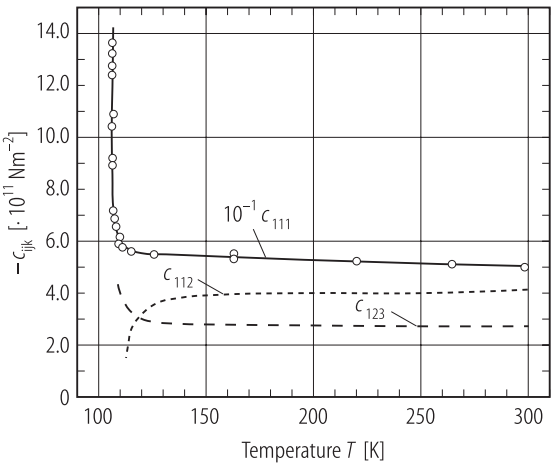

Fig. 1A-8-065. $SrTiO_3$. c_{ijk} vs. T [70Mee]. c_{ijk}: third order elastic constant determined on the assumption of extended Cauchy relations above 102.5 K. See also [71Pet].

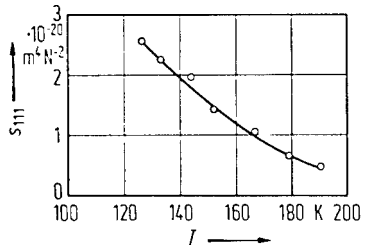

Fig. 1A-8-066. $SrTiO_3$. s_{111} vs. T [74Sor]. s_{111}: third order compliance coefficient determined from the shift of resonant frequency with increasing amplitude of driving electric field.

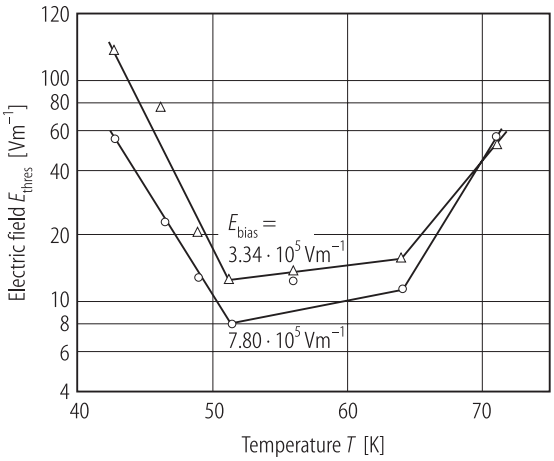

Fig. 1A-8-067. $SrTiO_3$. E_{thres} vs. T [70Sor2]. Parameter: E_{bias}. E_{thres}: threshold field for nonlinear response (instability).

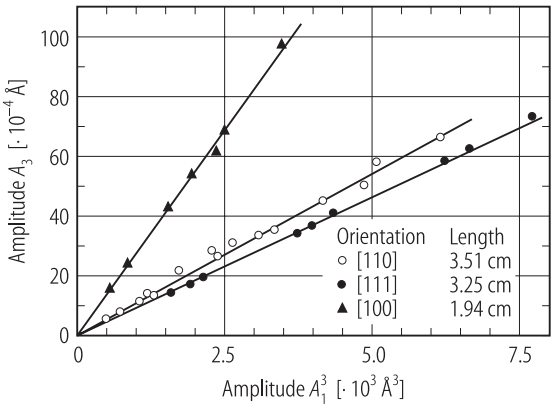

Fig. 1A-8-068. $SrTiO_3$. A_3 vs. 71Pet]. Third-harmonic generation of sound. Parameter: crystal orientation. A_3: third harmonic amplitude, A_1: fundamental amplitude (20 MHz). Amplitudes were measured using a capacitive detector. Temperature: RT.

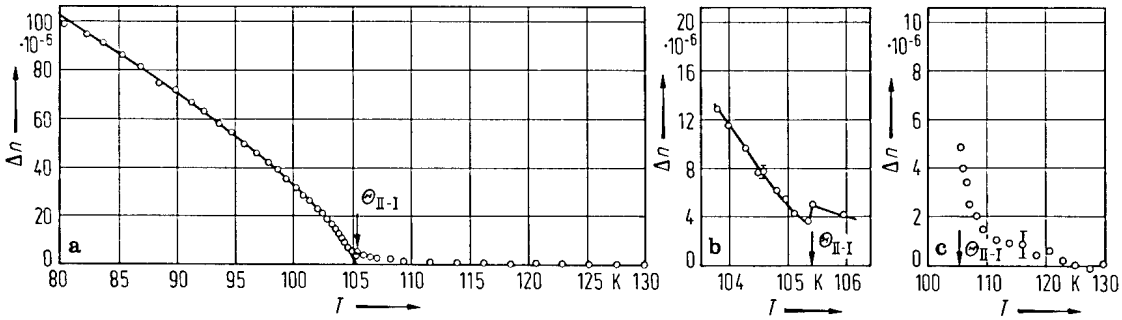

Fig. 1A-8-069. $SrTiO_3$. Δn vs. T [72Cou]. Temperature range of measurement: **(a)** entire range (80...130 K), **(b)** in the vicinity of Θ_{II-I}, **(c)** above Θ_{II-I} (with expanded vertical scale). λ = 632.8 nm.

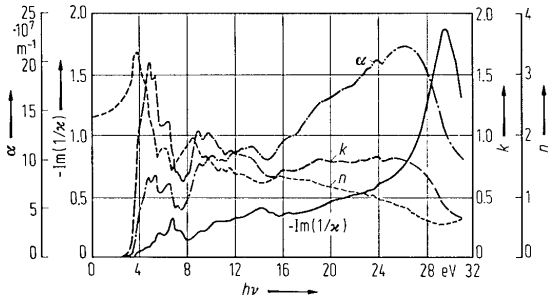

Fig. 1A-8-070. $SrTiO_3$. −Im (1/κ), *n*, *k*, α vs. $h\nu$ [78Bau]. Im (1/κ): loss function, *n*: real part of refractive index, *k*: imaginary part of refractive index, α: absorption coefficient.

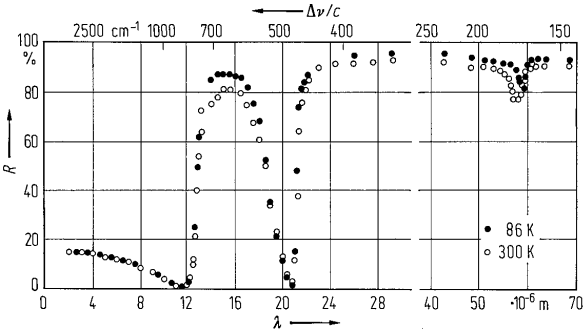

Fig. 1A-8-071. $SrTiO_3$. R vs. λ [66Bar]. R: reflectivity, λ: wavelength of incident infrared radiation. Polarization of the light is not specified.

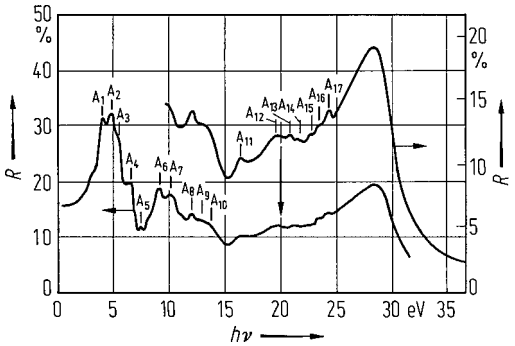

Fig. 1A-8-072. $SrTiO_3$. *R* vs. $h\nu$ [78Bau]. *R* for $h\nu < 10$ eV from[65Car].
R: reflectivity. A vertical arrow marks the expected onset of Sr 4p to conduction band transition. Labeling is as follows; for the labeling in parentheses, see [65Car].

Labeling	Energy [eV]	Labeling	Energy [eV]	Labeling	Energy [eV]
E_0	3.4	A_6 (C_1)	9.2	A_{12}	19.6
A_1 (A_1)	4.0	A_7 (C_2)	10.2 (9.9)	A_{13}	20.8
A_2 (A_2)	4.86	A_8	12.0	A_{14}	21.6
A_3 (A_3)	5.5	A_9	13.0	A_{15}	22.8
A_4 (B_1)	6.52	A_{10}	13.8	A_{16}	23.4
A_5 (B_2)	7.4	A_{11}	16.4	A_{17}	24.3

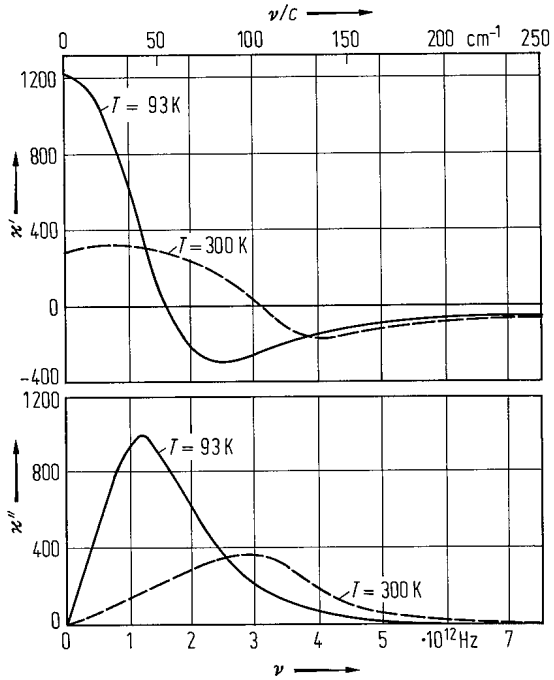

Fig. 1A-8-073. $SrTiO_3$. κ', κ'' vs. ν [62Bar]. Parameter: *T*. Results are obtained by Kramers-Kronig analysis from reflectivity data.

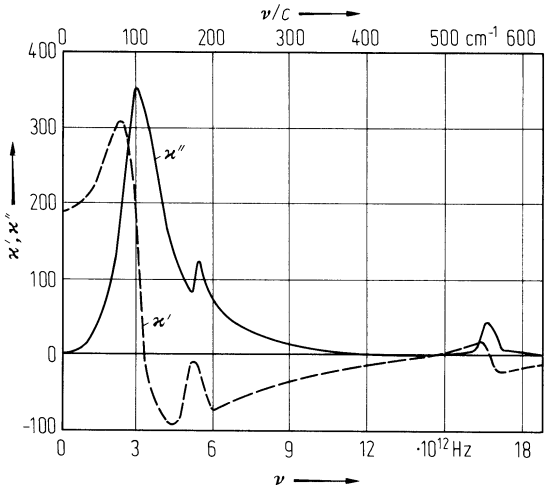

Fig. 1A-8-074. $SrTiO_3$. κ ', κ " vs. ν [64Per]. T = RT. Results are obtained by Kramers-Kronig analysis from reflectivity data.

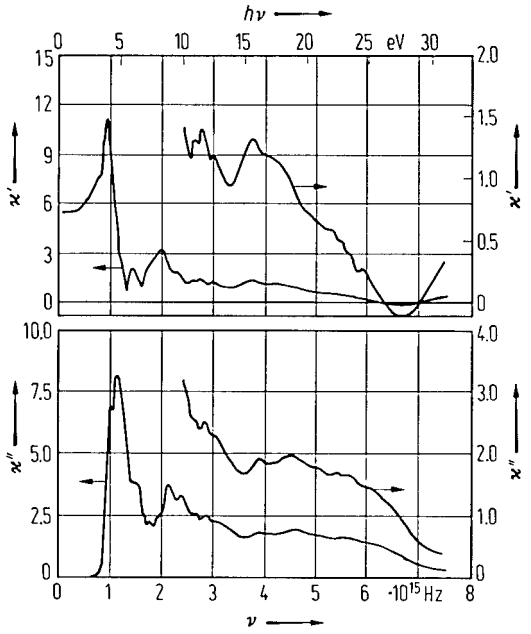

Fig. 1A-8-075. $SrTiO_3$. κ', κ'' vs. ν [78Bau]. Ultraviolet region. Results are obtained by Kramers-Kronig analysis from reflectivity data.

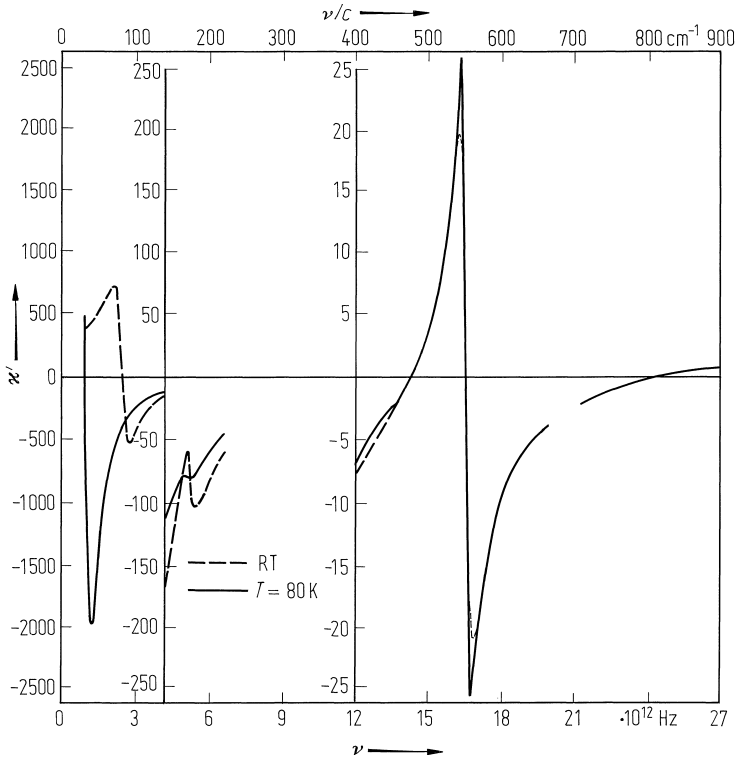

Fig. 1A-8-076. $SrTiO_3$. κ' vs. ν [82Gal]. Parameter: *T*. Curves were obtained from the fit of unpolarized light reflectivity data to a coupled oscillator model. Note that the scale of ordinate changes at $4.2 \cdot 10^{12}$ and $12 \cdot 10^{12}$ Hz.

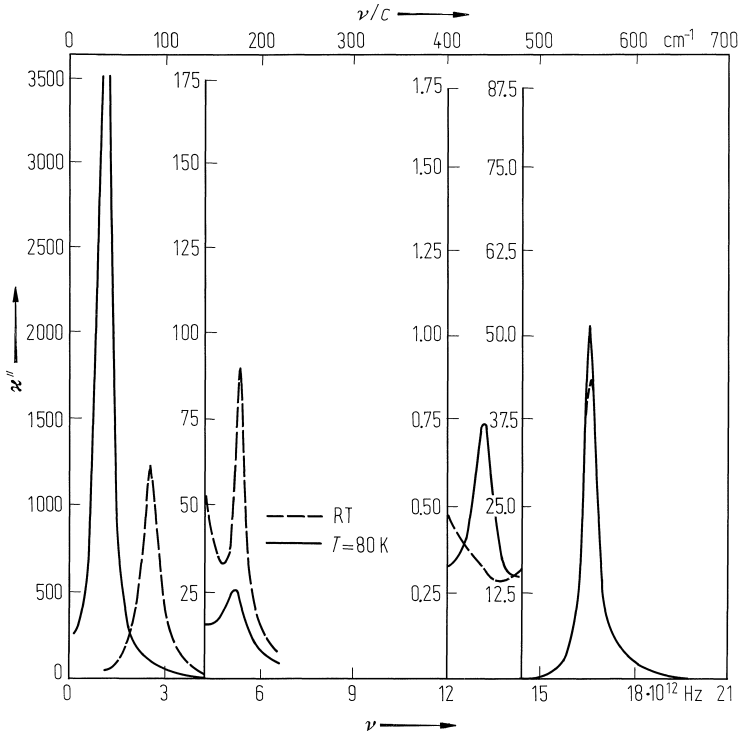

Fig. 1A-8-077. $SrTiO_3$. κ " vs. ν [82Gal]. Parameter: *T*. The coupled oscillator model was used as described in the caption of **Fig**. 1A-8-076.

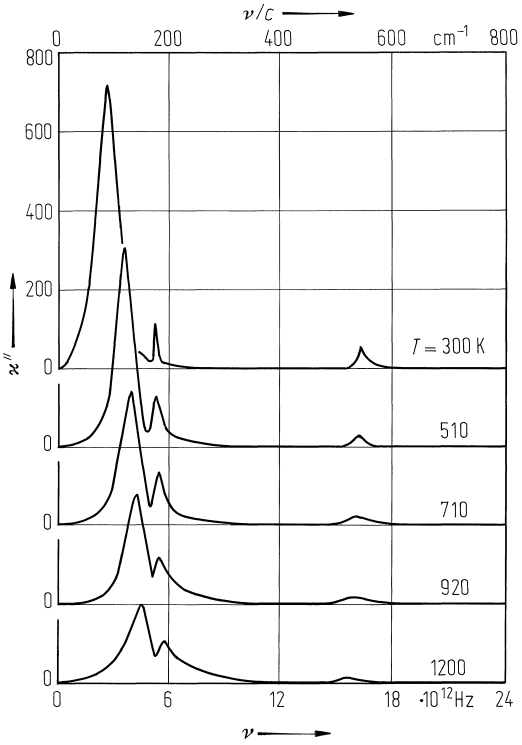

Fig. 1A-8-078. $SrTiO_3$. κ'' vs. ν [80Ser]. Parameter: T. ν: frequency in infrared region. Curves were obtained by Kramers-Kronig analysis from reflectivity data.

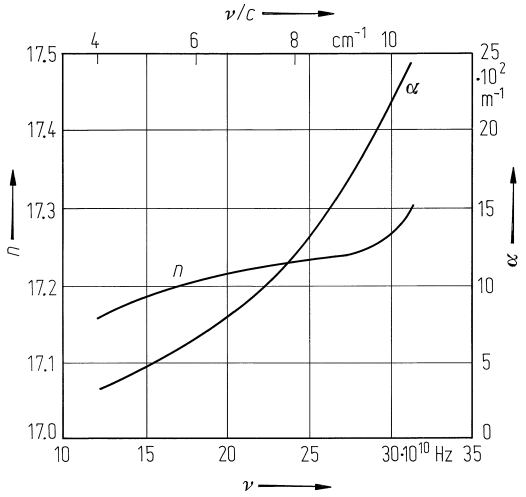

Fig. 1A-8-079. $SrTiO_3$. n, α vs. ν [83Bro]. n: refractive index, α: power absorption coefficient, ν: frequency in near-mm wave region.

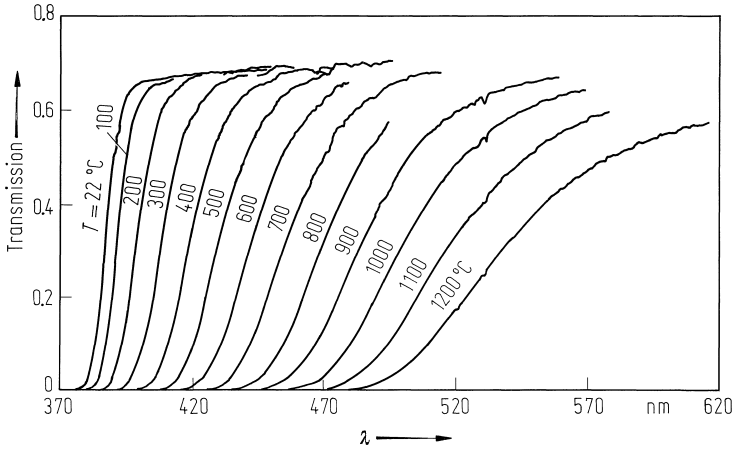

Fig. 1A-8-080. $SrTiO_3$. Optical transmission vs. λ [87Gol]. Parameter: *T*. Sample thickness: 117 μm.

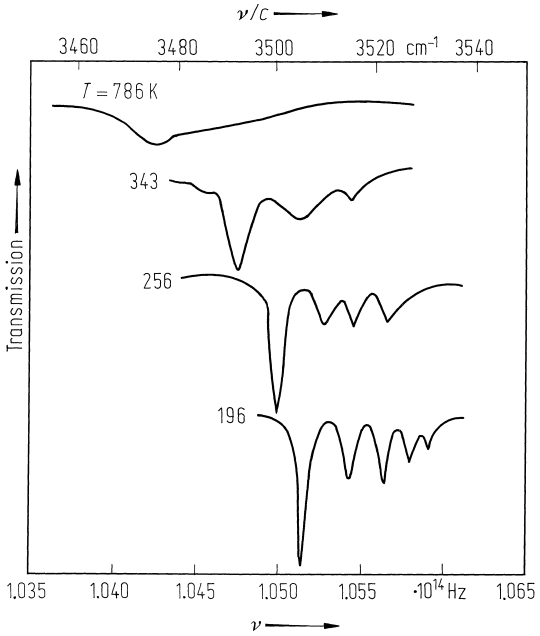

Fig. 1A-8-081. $SrTiO_3$. Infrared transmission vs. ν [87Hou]. Parameter: T (>190 K). Measurement was made at frequencies around O-H stretching vibration frequency. Single crystal samples contain hydrogen impurity.

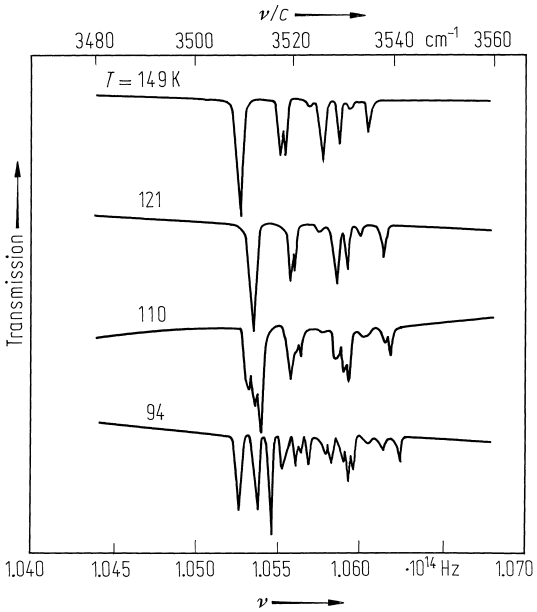

Fig. 1A-8-082. $SrTiO_3$. Infrared transmission vs. ν [87Hou]. Parameter: T (90 K < T < 190 K). Frequency range is nearly the same as in **Fig**. 1A-8-081.

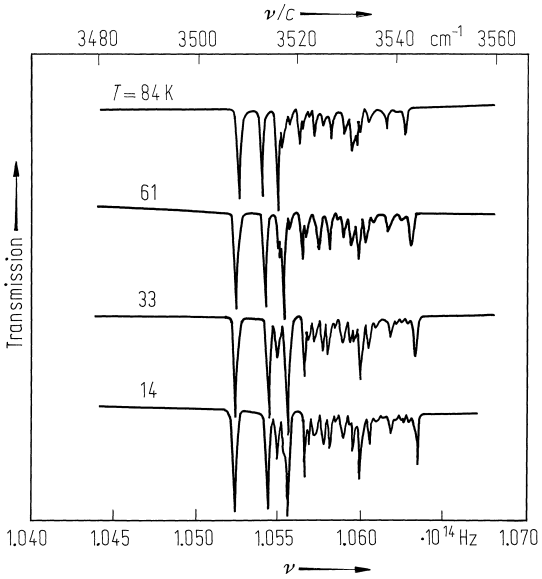

Fig. 1A-8-083. $SrTiO_3$. Infrared transmission vs. ν [87Hou]. Parameter: T (< 90 K). Frequency range is nearly the same as in **Fig**. 1A-8-081.

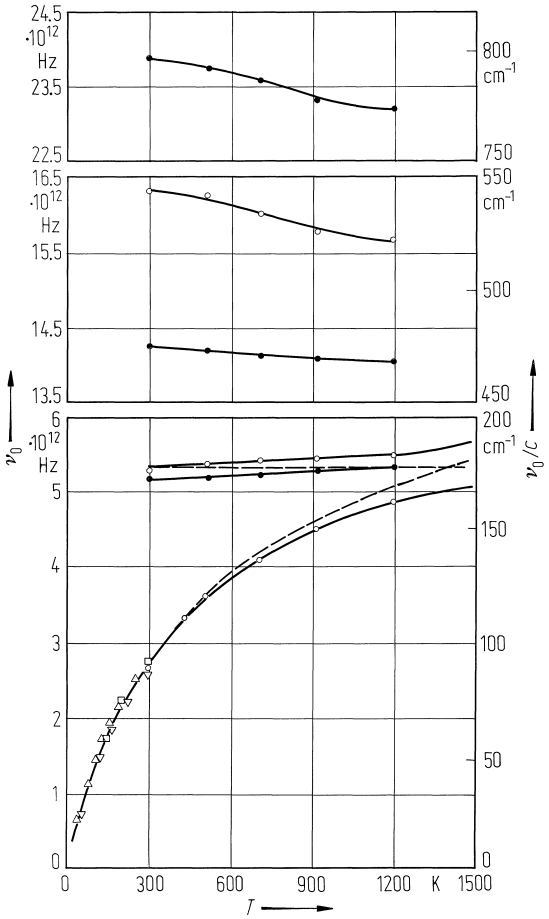

Fig. 1A-8-084. $SrTiO_3$. ν_0 vs. T [80Ser]. ν_0: lattice vibration frequencies determined from infrared reflection spectra. Open circles: TO-mode, solid circles: LO-mode; for other symbols, see references in the original paper. Dashed curves are decoupled mode frequencies.

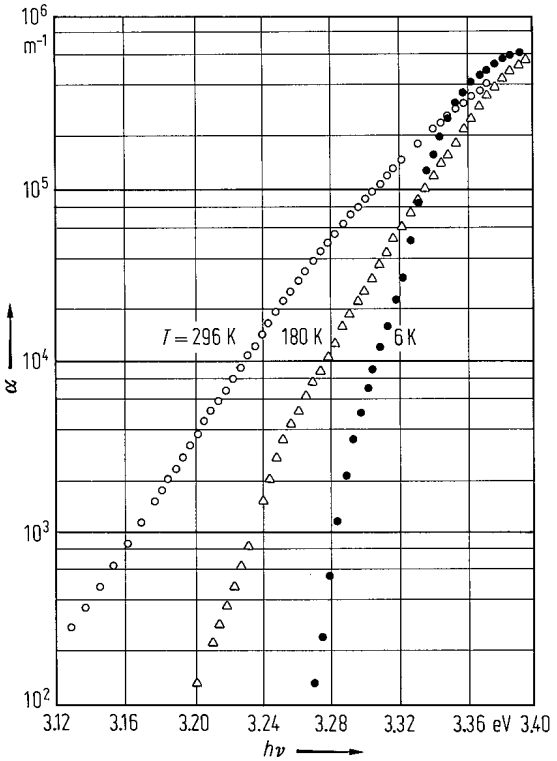

Fig. 1A-8-085. $SrTiO_3$. α vs. $h\nu$ [72Red]. Parameter: T.

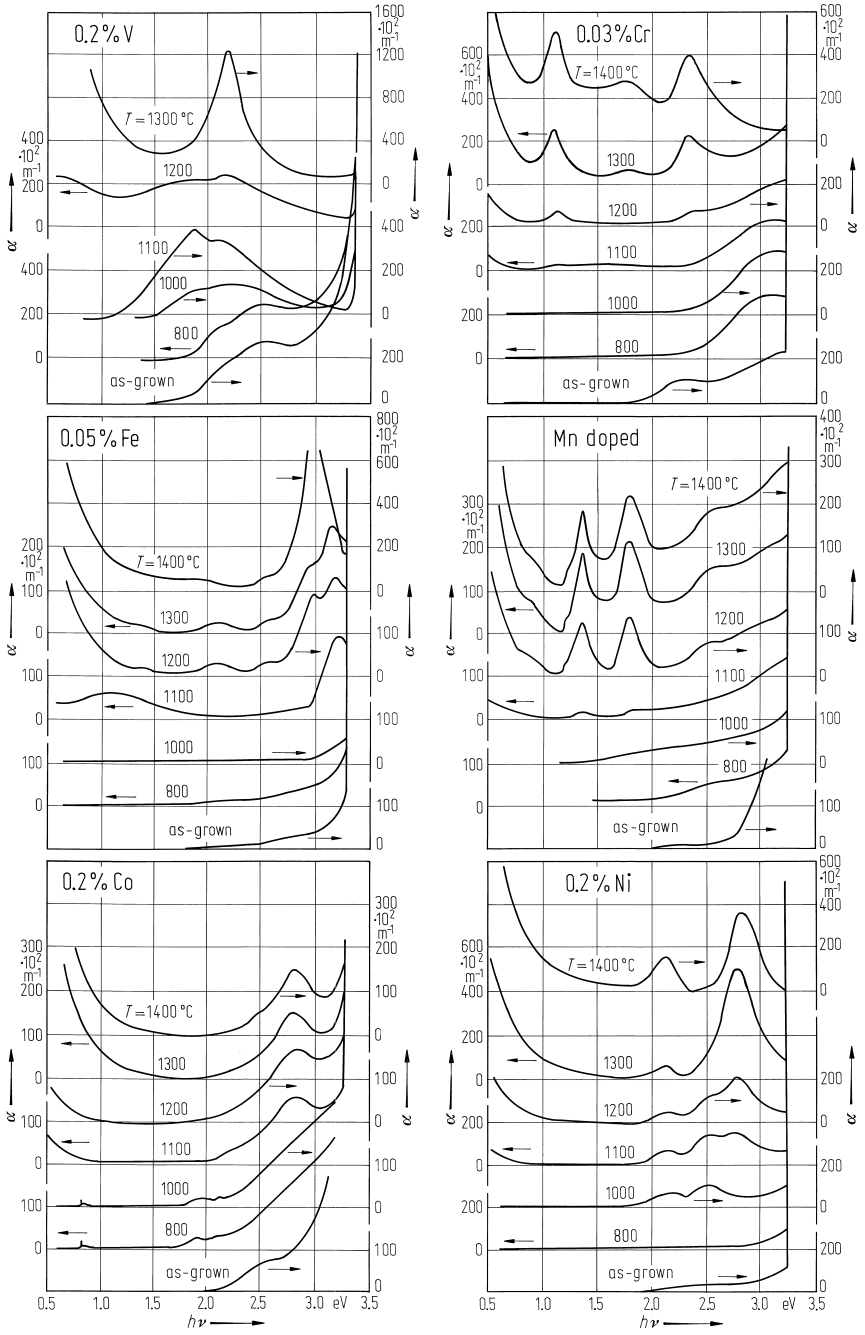

Fig. 1A-8-086. $SrTiO_3$ doped with transition metals. α vs. $h\nu$ [84Bla]. Parameter: T (reduction temperature of the sample). α: optical absorption. Note that zero point of α scale is arbitrary. Dopant and its concentration are indicated in the **fig**ure.

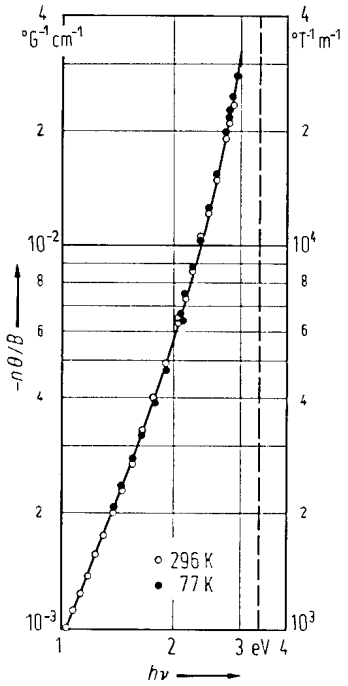

Fig. 1A-8-087. $SrTiO_3$. $-n\theta / B$ vs. $h\nu$ [67Bae]. n: refractive index, θ: interband Faraday rotation per unit length, B: magnetic induction. Solid line is a fit to dispersion function $F_1(\omega / \omega_g)$. Dashed line shows band gap energy E_g = 3.40 eV.

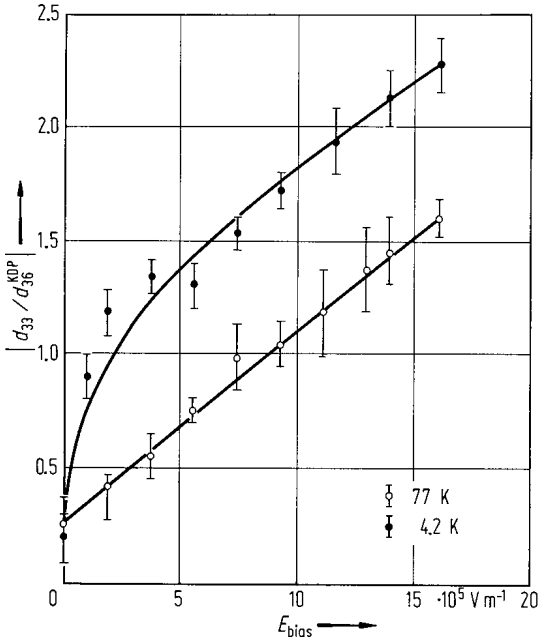

Fig. 1A-8-088. $SrTiO_3$. $\left|d_{33}/d_{36}^{KDP}\right|$ vs. E_{bias} [70Sak]. d_{ijk}: nonlinear optical susceptibility. Solid curves are the induced polarization fitted at $E = 0$ and $E = 16 \cdot 10^5$ V m^{-1}.

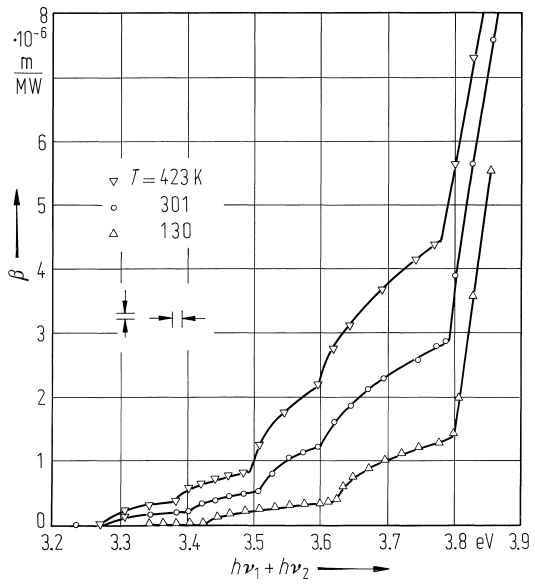

Fig. 1A-8-089. $SrTiO_3$. β vs. $h\nu_1$ + $h\nu_2$ [84Sha]. Parameter: *T*. β: two-photon absorption coefficient. $h\nu_1$ = 1.17 eV for neodymium laser pump radiation, $h\nu_2$ for probe light from a xenon pulse discharge lamp. See also [79Sha].

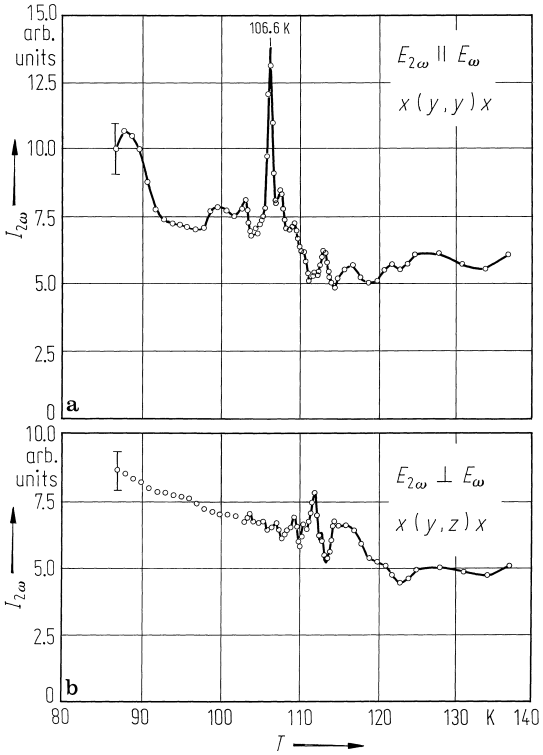

Fig. 1A-8-090. $SrTiO_3$. $I_{2\omega}$ vs. T [80Bet]. $I_{2\omega}$: Intensity of SHG (second harmonic generation) for incident beam with λ = 1.060 nm. Polarization of SHG: **(a)** parallel to the polarization of incident beam, **(b)** perpendicular to that.

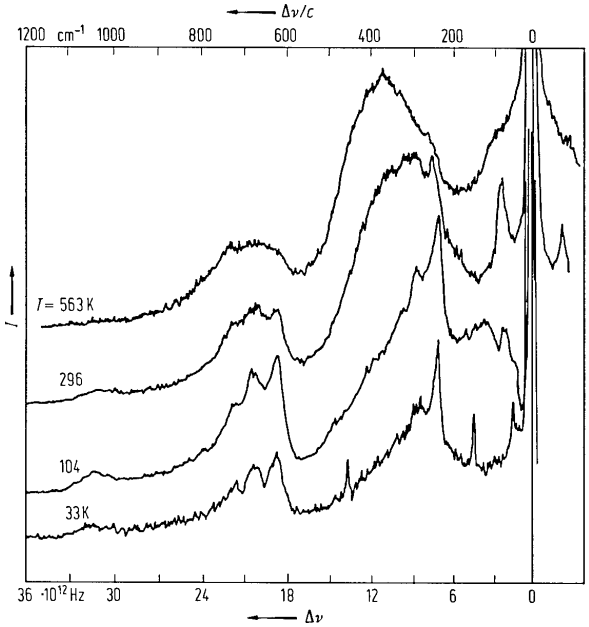

Fig. 1A-8-091. $SrTiO_3$. I vs. $\Delta\nu$ [67OSh]. Parameter: T. I: Raman scattering intensity, $\Delta\nu$: frequency shift. Polarization of the light is not specified. See also [68Fle2].

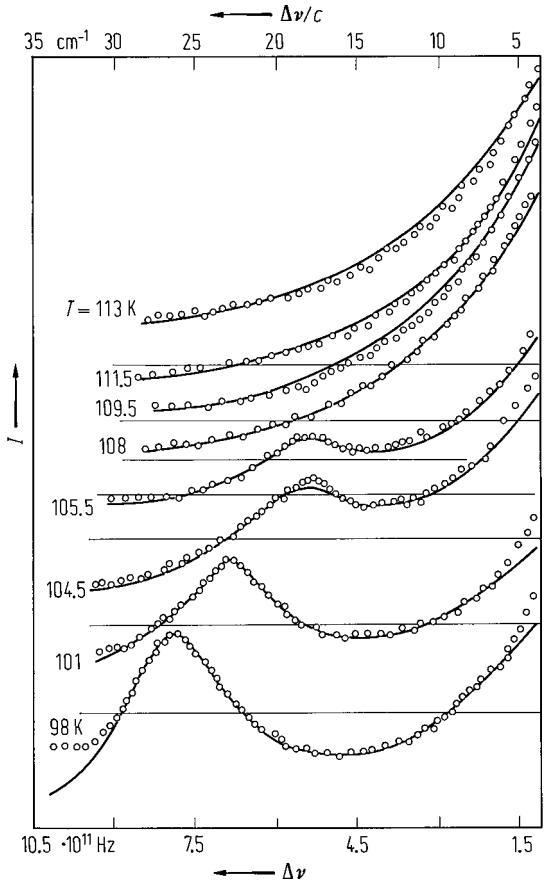

Fig. 1A-8-092. $SrTiO_3$. I vs. $\Delta\nu$ [76Fir]. Parameter: T (near 110 K transition). I: Raman scattering intensity of the lowest A_{1g} mode, $\Delta\nu$: frequency shift. Solid lines show calculated spectra.

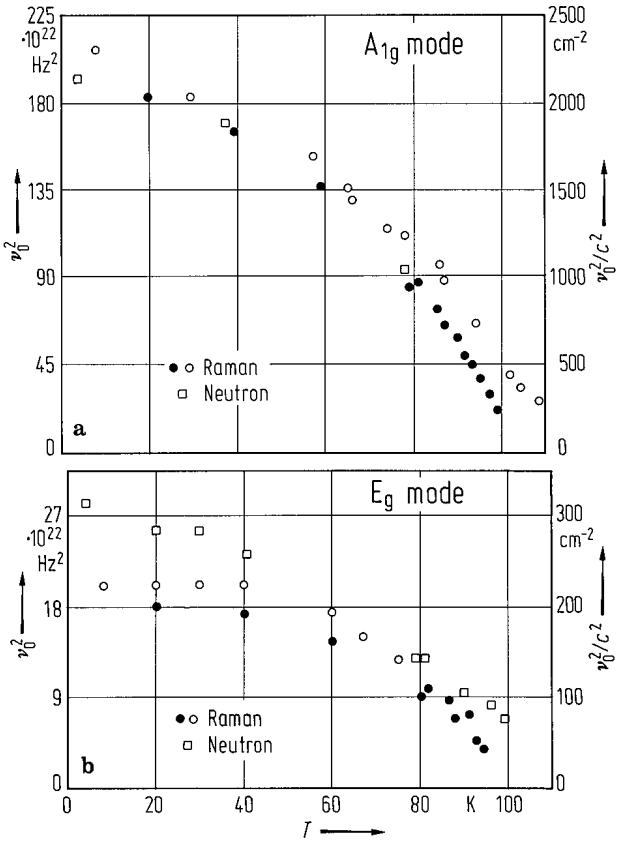

Fig. 1A-8-093. $SrTiO_3$. ν_0^2 vs. T [71Wor]. ν_0^2: soft mode frequency of A_{1g} mode **(a)** and E_g mode **(b)**. Solid and open circles are the results from Raman spectra [71Wor], [68Fle1]. Squares are the results of neutron diffraction [69Shi].

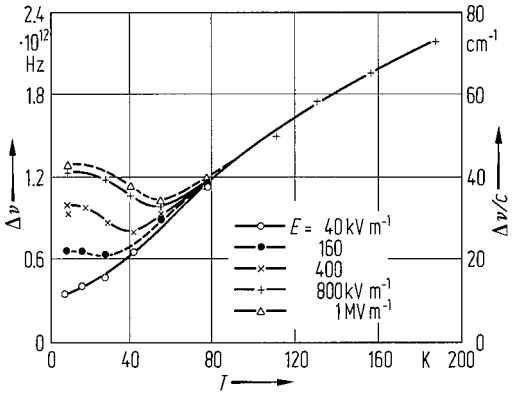

Fig. 1A-8-094. $SrTiO_3$. $\Delta\nu$ vs. T [68Fle2]. Parameter: E. $\Delta\nu$: Raman frequency shift, E: electric field in <001> direction.

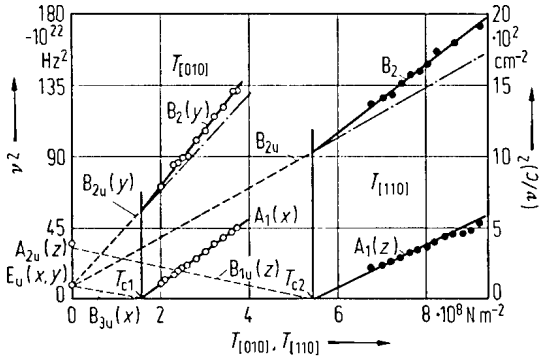

Fig. 1A-8-095. $SrTiO_3$. ν^2 vs. $T_{[010]}$, $T_{[110]}$ [76Uwe]. ν: frequency of soft mode. $T_{[010]}$, $T_{[110]}$: uniaxial stress perpendicular to (010) and (110), respectively. Open circles: data for $T_{[010]}$, full circles: data for $T_{[110]}$. Dashed lines below critical stress T_{c1} and T_{c2} and dots at $T = 0$ were calculated using dielectric and electrostrictive constants. $T = 2$ K.

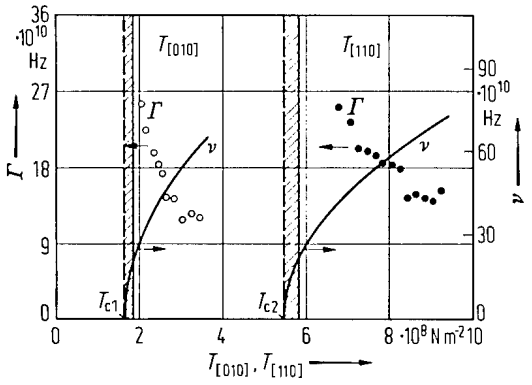

Fig. 1A-8-096. $SrTiO_3$. ν, Γ vs. $T_{[010]}$, $T_{[110]}$ [76Uwe]. ν: frequency of A_1 symmetry mode. Γ: damping constant of the mode. $T_{[010]}$, $T_{[110]}$: uniaxial stress perpendicular to (010) and (110), respectively. Open circles: data for $T_{[010]}$, full circles: data for $T_{[110]}$. Shaded ranges near T_{c1} and T_{c2} indicate overdamped region ($\Gamma > 2\nu$). $T = 2$ K.

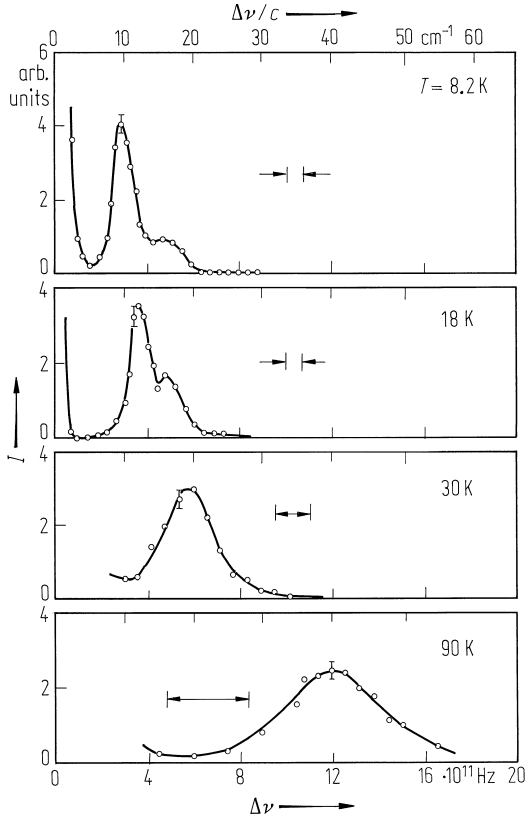

Fig. 1A-8-097. $SrTiO_3$. I vs. $\Delta\nu$ [81Ino]. Parameter: T. I: hyper-Raman scattering intensity of the soft TO mode observed in the forward direction, $\Delta\nu$: Raman shift. Ordinate scale is arbitrary and different among four curves. Instrumental resolution is indicated by the respective horizontal bar.

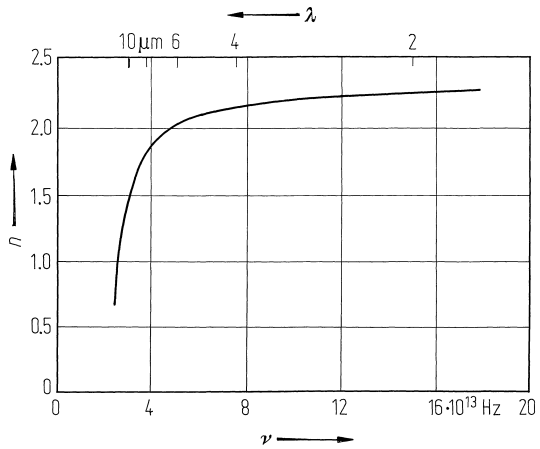

Fig. 1A-8-098. $SrTiO_3$. *n* vs. *ν* [80Den]. *n*: refractive index obtained from hyper-Raman scattering experiment.

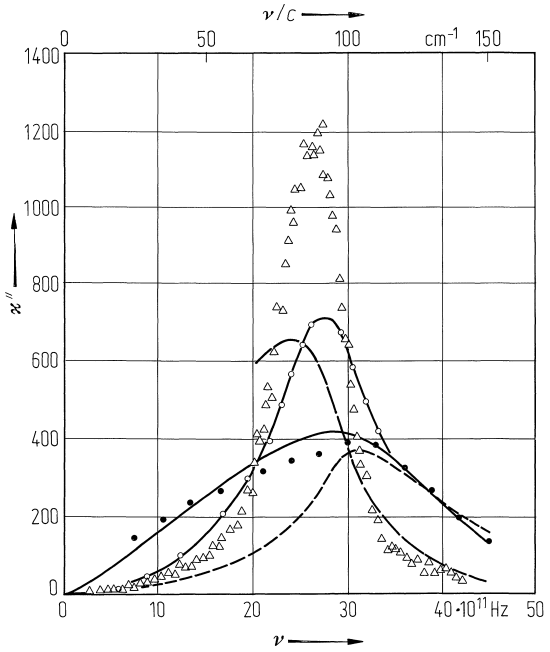

Fig. 1A-8-099. $SrTiO_3$. κ'' vs. ν [81Vog]. Triangles were obtained from hyper-Raman spectrum. Other marks and curves are the results of previous infrared studies; see the original paper. T = RT.

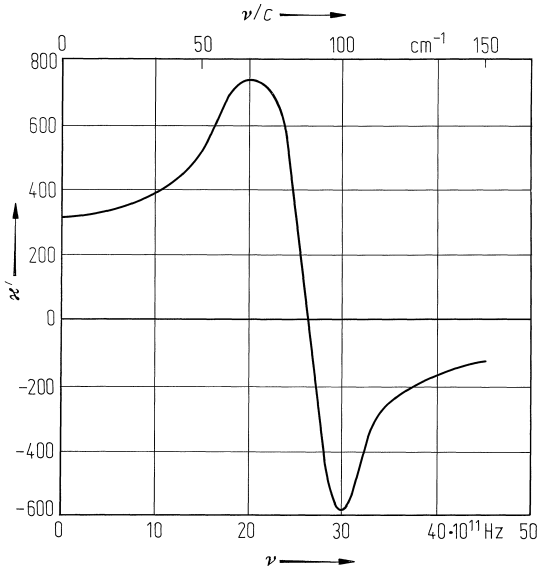

Fig. 1A-8-100. $SrTiO_3$. κ' vs. ν [81Vog]. Kramers-Kronig transformation was applied on κ'' obtained from hyper-Raman spectrum (see **Fig**. 1A-8-99), and that from infrared study [62Spi] was incorporated.

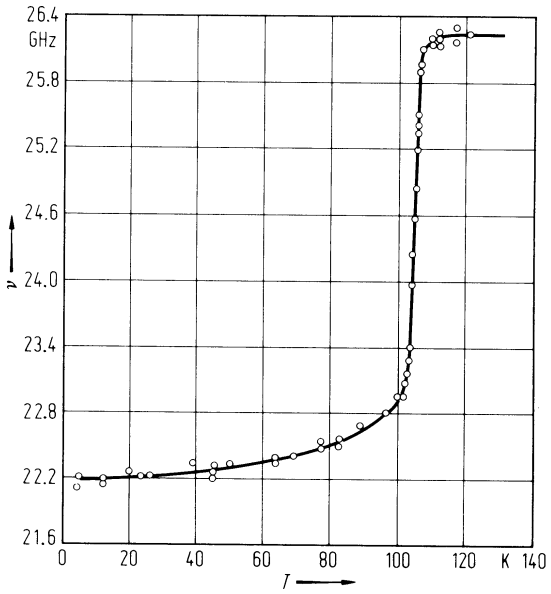

Fig. 1A-8-101. $SrTiO_3$. ν vs. T [70Lau]. ν: Brillouin frequency shift of the transverse acoustic wave propagated along [100] with the polarization normal to the scattering plane (001). Scattering angle: 90^o.

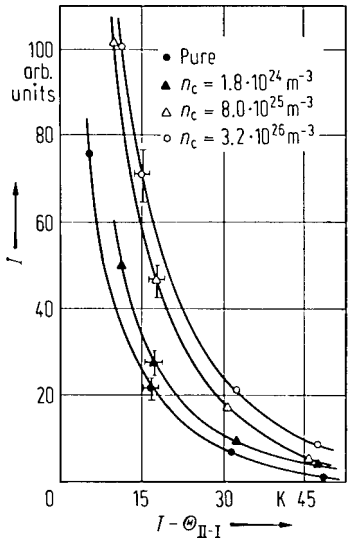

Fig. 1A-8-102. $SrTiO_3$ (hydrogen reduced). I vs. $T-\Theta_{II-I}$ [78Has]. Parameter: n_c. I: Integrated intensity of a central peak (in arbitrary scale), n_c: carrier density. "Pure" stands for unreduced reference sample ($n_c \approx 1 \cdot 10^{24}$ m^{-3}).

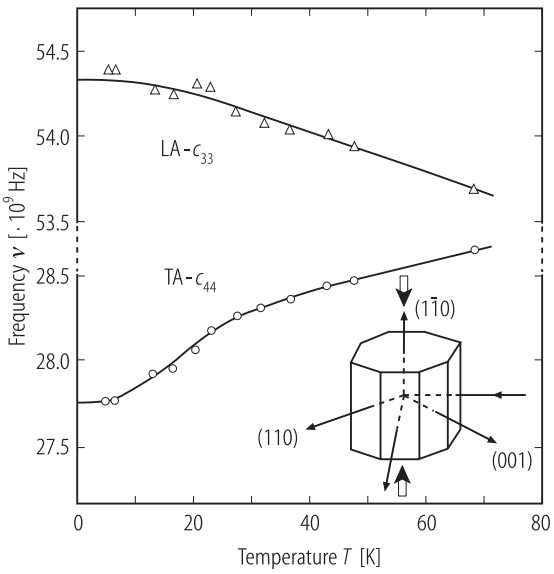

Fig. 1A-8-103. $SrTiO_3$. ν vs. T [93Cou]. ν: Brillouin frequency for modes propagated along c-axis (with wave vector $\boldsymbol{q}$ ‖ [001]). LA: longitudinal acoustic branch, TA: transverse acoustic branch. Insert shows experimental con**fig**uration, where the probing beam enters from the right face and the scattered light is observed from the front. Compressional stress of $4 \cdot 10^7$ N m^{-2} is applied in vertical direction.

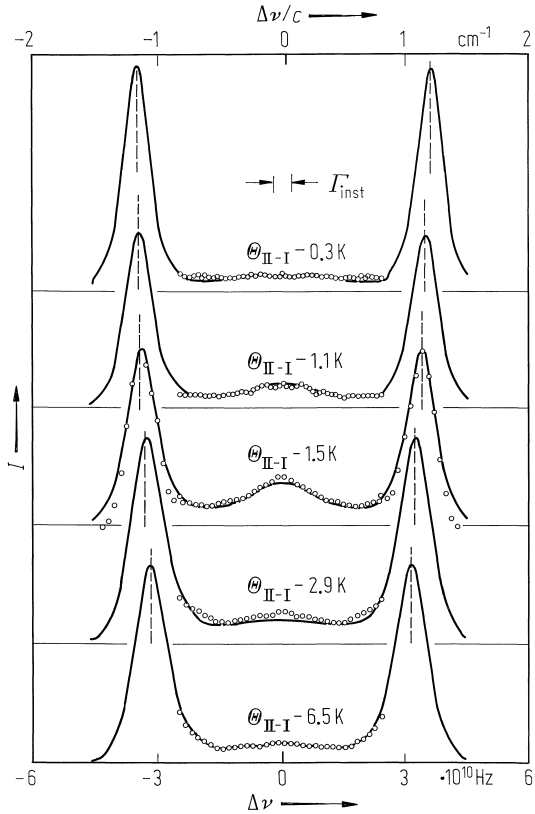

Fig. 1A-8-104. $SrTiO_3$. I vs. $\Delta\nu$ [79Fle]. I: intensity of depolarized central peak near Θ_{II-I}. $\Delta\nu$: Brillouin scattering frequency shift. Solid curves are fits to a model calculation. Γ_{inst} indicates instrumental half-width at half maximum. λ = 514.5 nm.

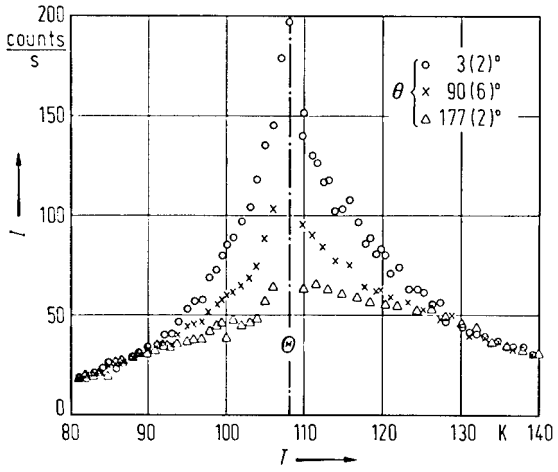

Fig. 1A-8-105. $SrTiO_3$. I vs. T [74Ste]. Parameter: θ. I: Raman scattering intensity, θ: scattering angle. Θ = 108.2 K.

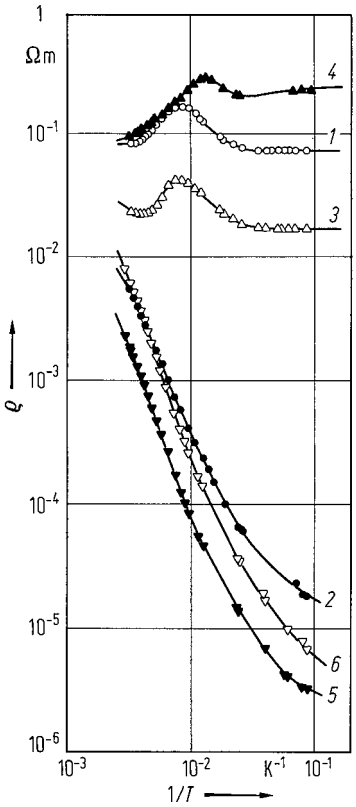

Fig. 1A-8-106. $SrTiO_3$. ρ vs. $1/T$ [75Lee]. ρ: electrical resistivity. For sample numbers, see Table 1A-8-007.

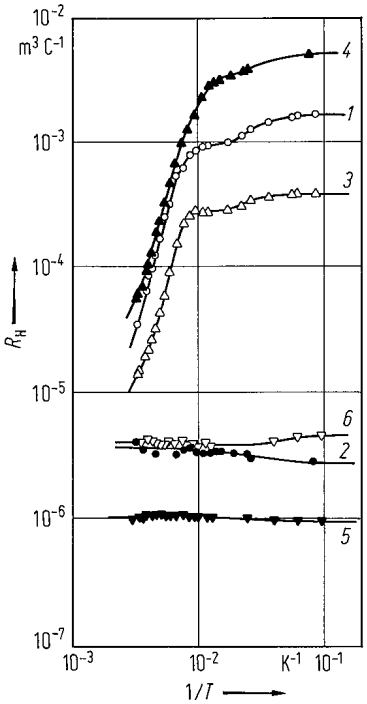

Fig. 1A-8-107. $SrTiO_3$. R_H vs. $1/T$ [75Lee]. R_H: Hall coefficient. For sample numbers, see Table 1A-8-007.

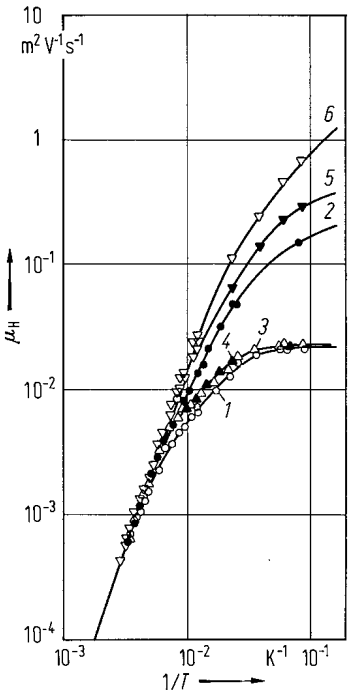

Fig. 1A-8-108. $SrTiO_3$. μ_H vs. $1/T$ [75Lee]. μ_H: Hall mobility. For sample numbers, see Table 1A-8-007.

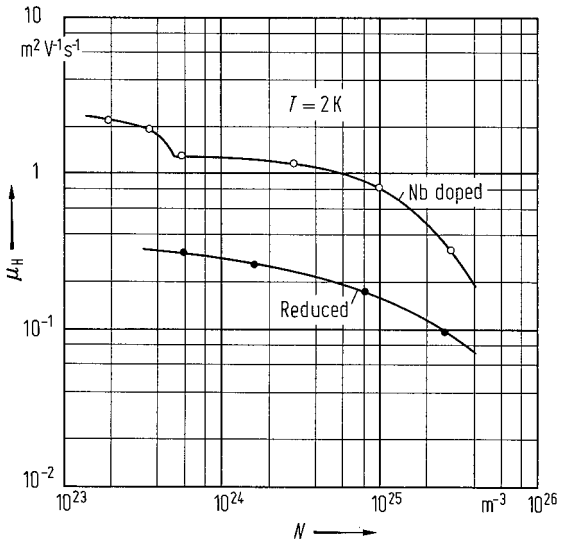

Fig. 1A-8-109. $SrTiO_3$ (semiconducting single crystal). μ_H vs. N [67Tuf]. μ_H: Hall mobility, N: electron concentration.

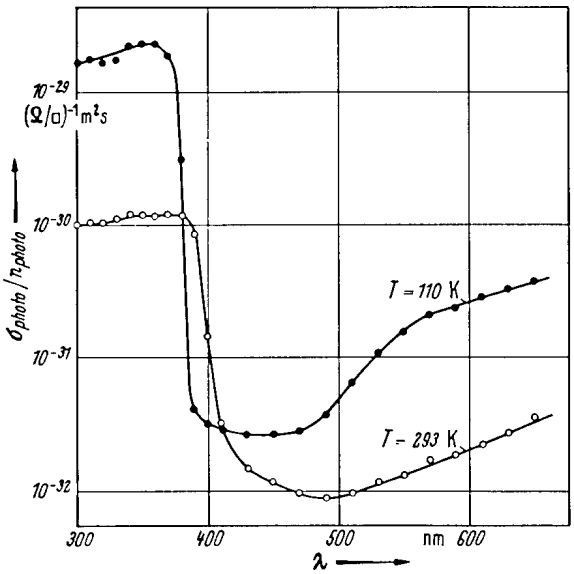

Fig. 1A-8-110. $SrTiO_3$. σ_{photo}/n_{photo} vs. λ [67Yas]. Parameter: T. σ_{photo}: surface photoconductivity, n_{photo}: photon density falling on the surface.

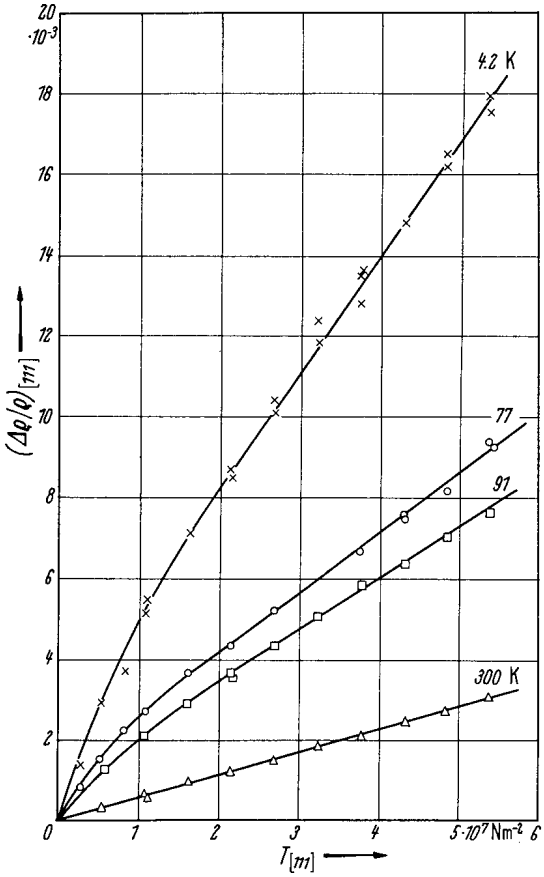

Fig. 1A-8-111. $SrTiO_3$ (semiconducting single crystal). $(\Delta\rho/\rho)_{[111]}$ vs. $T_{[111]}$ [66Tuf]. Parameter: T. $(\Delta\rho/\rho)_{[111]}$: longitudinal piezoresistive effect, $T_{[111]}$: compressive stress along [111]. $\rho = 2.9 \cdot 10^{-4}\ \Omega$m at RT.

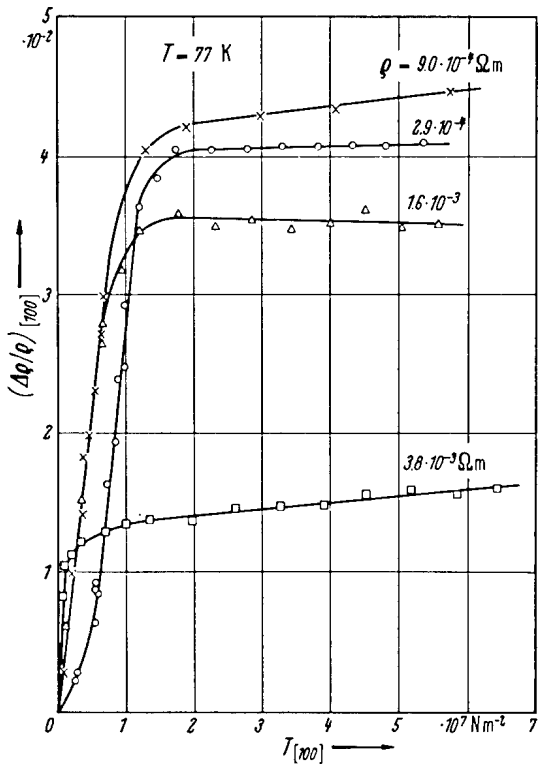

Fig. 1A-8-112. $SrTiO_3$ (semiconducting single crystal). $(\Delta\rho/\rho)_{[100]}$ vs. $T_{[100]}$ [66Tuf]. Parameter: ρ. $(\Delta\rho/\rho)_{[100]}$: longitudinal piezoresistive effect, $T_{[100]}$: compressive stress along [100]. Value of ρ refers to RT for each sample. T = 77 K.

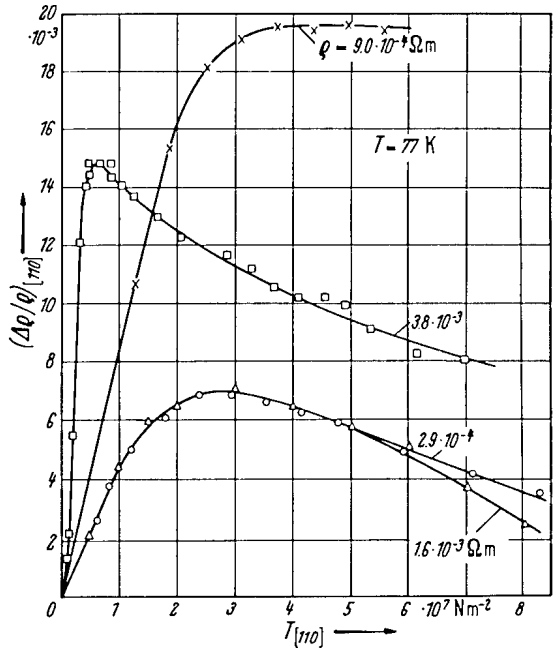

Fig. 1A-8-113. $SrTiO_3$ (semiconducting single crystal). $(\Delta\rho/\rho)_{[110]}$ vs. $T_{[110]}$ [66Tuf]. Parameter: ρ. $(\Delta\rho/\rho)_{[110]}$: longitudinal piezoresistive effect, $T_{[110]}$: compressive stress along [110]. Value of ρ refers to RT for each sample. T = 77 K.

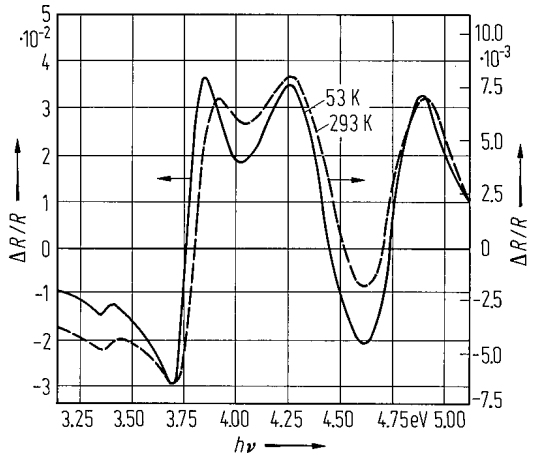

Fig. 1A-8-114. $SrTiO_3$. $\Delta R/R$ vs. $h\nu$ [74Mac]. $\Delta R/R$: electroreflectance for unpolarized light. Square wave ac field with 2V peak-to-peak was applied in <110> direction.

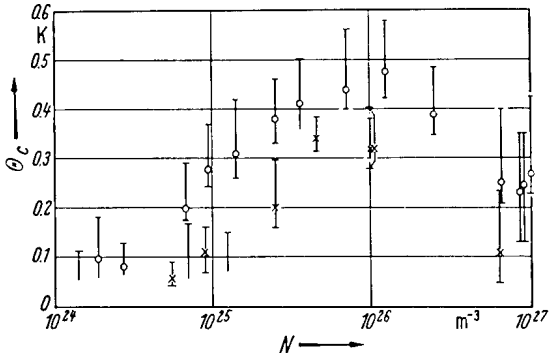

Fig. 1A-8-115. $SrTiO_3$ (reduced). Θ_c vs. N [65Sch]. Θ_c: superconducting transition temperature, N: charge carrier concentration. Circles and crosses indicate midpoints of resistive transition and those of magnetic transitions, respectively. Vertical bars denote temperature range of the respective transitions.

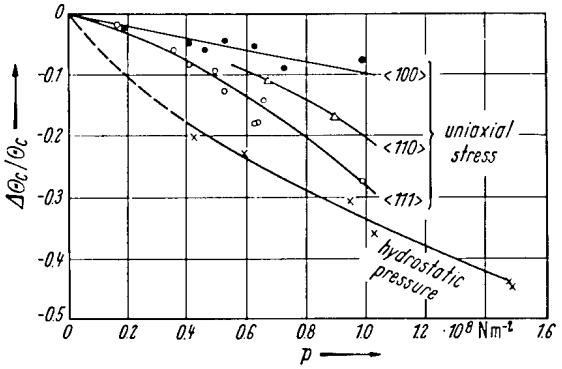

Fig. 1A-8-116. $SrTiO_3$ (reduced). $\Delta\Theta_c/\Theta_c$ vs. p [67Pfe]. Parameter: character of stress. $\Delta\Theta_c/\Theta_c$: change of superconducting transition temperature, p: uniaxial stress or hydrostatic pressure. $\Theta_c \approx 0.27$ K at $p = 0$, charge carrier concentration = $6.3 \cdot 10^{25}$ m^{-3}.

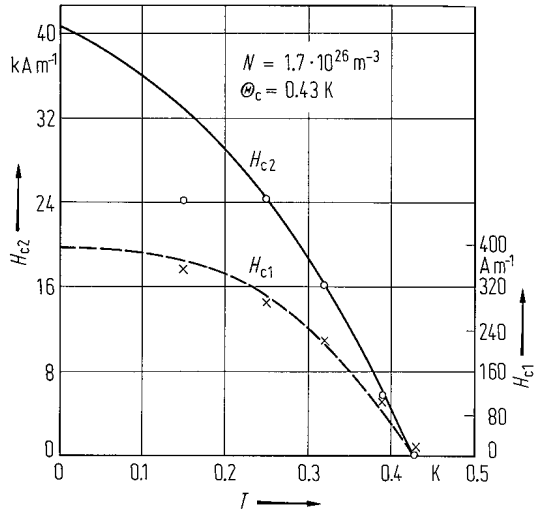

Fig. 1A-8-117. $SrTiO_3$ (Nb-doped). H_{c1}, H_{c2} vs. T [66Amb]. H_{c1}: the field strength at which the M–H curve first deviates from linearity, H_{c2}: the intercept of the M–H curve with the M-axis. Carrier concentration $N = 1.7 \cdot 10^{26}$ m^{-3}, superconducting temperature $\Theta_c = 0.43$ K.

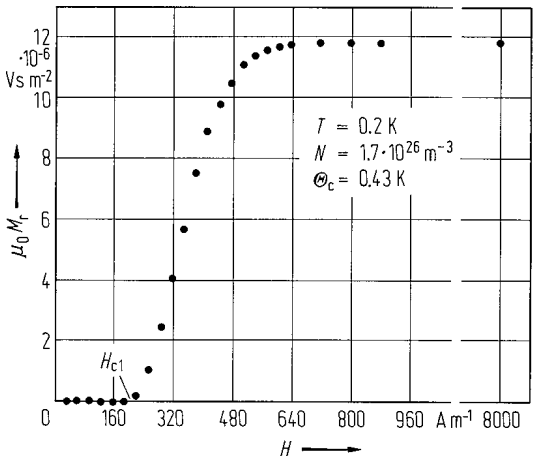

Fig. 1A-8-118. $SrTiO_3$ (Nb-doped). $\mu_0 M_r$ vs. H [66Amb]. M_r: residual magnetization after removal of magnetic field at 0.2 K. About H_{c1}, N and Θ_c see **Fig**. 1A-8-117. Ordinate scale has to be multiplied by a factor 4π to get true values of $\mu_0 M_r$.

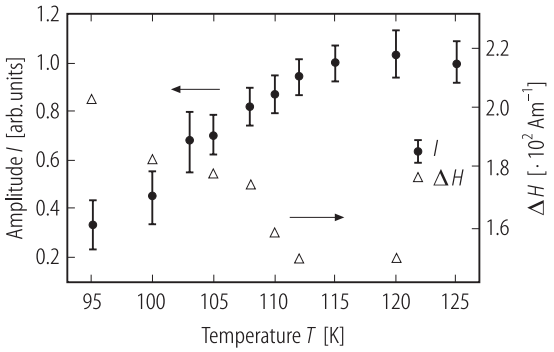

Fig. 1A-8-119. $SrTiO_3$. I, ΔH vs. T [63Web]. NMR of ^{87}Sr. I: peak amplitude (full circles), ΔH: line width (open triangles).